Lower Thermosphere response to solar activity: an EMD analysis of GOCE 2009-2012 data.

Alberto Bigazzi[1], Carlo Cauli[1], and Francesco Berrilli[1]

[1]University of Rome Tor Vergata, Via della Ricerca Scientifica, 1, Roma, ITALY

Correspondence: Alberto Bigazzi (alberto.bigazzi@roma2.infn.it)

Abstract. Forecasting the Thermosphere (Atmosphere's uppermost layer, from about 90 to 800 km altitude) is crucial to space-related applications, from space mission design, to re-entry operations, space surveillance and more. Thermospheric dynamics is directly linked to the solar dynamics through the solar UV input, which is highly variable, and through the solar wind and plasma fluxes, impacting Earth's magnetosphere. The solar input is non-periodic and non-stationary, with long-term modulations from the solar rotation and the solar cycle, and impulsive components, due to magnetic storms. Proxies of the solar input exist and may be used to forecast the thermosphere, such as the F10.7 radio flux and the MgII EUV flux. They relate to physical processes on the Solar atmosphere. Other indices, such as the A_p geomagnetic index, connect with Earth's geomagnetic environment. We analyse the proxies' time series comparing them with in-situ density data from the ESA/GOCE gravity mission, operational from March 2009 to November 2013, therefore covering the full rising phase of solar cycle XXIV, exposing the entire dynamic range of the solar input. We use Empirical Mode Decomposition (EMD), an analysis technique appropriate to non-periodic, multi-scale signals. Data are taken at an altitude of 260 km, exceptionally low for a LEO satellite, where density variations are the single most important perturbation to satellite dynamics.

We show that the synthesized signal from optimally selected combinations of proxies's basis functions, notably MgII for the solar flux and Ap for the plasma component, show a very good agreement with thermospheric data obtained by GOCE, during low and medium solar activity periods. In periods of maximum solar activity, density enhancements are also well represented. The Mg II index proves to be, in general, a better proxy than the F10.7 one, to model the solar flux, because of its specific response to the UV spectrum, whose variations have the largest impact over thermospheric density.

1 Introduction

Forecasting the Thermosphere is crucial to space mission design, re-entry operations and space surveillance applications. Most low-Earth-Orbit operational satellites fly in a narrow zone between 400 and 800 km, within this layer. Orbital decay rate of Satellites depends on atmospheric drag which is directly affected by the variable solar activity (Masutti et al., 2016). Orbital decay rate at 250km of altitude is very significant, causing re-entry of a satellite in about two weeks. Large uncertainties in

the determination of satellite impact location during re-entry, results from the uncertainty in the knowledge of thermospheric density. During de-orbiting of GOCE, for instance, two hours before re-entry, the most probable ground impact area was still extending over the entire descending orbit, across the Pacific and Indian Oceans. (GOCE Flight Control Team, HSO-OEG, 2011). An impact over Europe could be ruled out just 12 hours before satellite disruption.

Various indices and proxies of the solar input are available, and used in monitoring and predicting the status of the Thermosphere. Most atmospheric density models have adopted the solar radio flux at 10.7 cm wavelength (the F10.7 index) as solar flux proxy (Floyd et al., 2005) and the Ap/Kp indices for geomagnetic activity (Omniweb, 2018). F10.7 has been measured daily since 1947 at Pentiction (Canada) at 17, 20 and 23 UTC. The Ap index instead provides 3-hourly averages of geomagnetic data. Other proxies and indices have been defined over time, some of them based on direct in-situ measurements from satellites, others derived from Earth-based obervatories. The Mg II core-to-wing ratio (cwr), has been provided daily since 1978 and is available through NOAA Space Environment Center or by the Institut für Umweltphysik - Universität Bremen (SORCE, 2018; UVSAT, 2018). The Mg II cwr has proved an excellent proxy for the solar Mid-UV. It originates from a chromospheric line emission near 280 nm. In particular, the chromospheric Mg II H and K lines at 279.56 and 280.27 nm, and the weakly varying photospheric wings continuum of the core line emission are observed by a number of on-board satellite instruments. Current semi-empirical models of the thermosphere, such as NRLMSISE-00 (Picone et al., 2002) and JB2008 (Bowman et al., 2008) include satellite drag data, mostly available between 400 and 600km height, and solar proxies. The NRL one includes, for instance, the F10.7 solar flux (present and averaged over the previous 81 days), and the Ap index for the previous 57-hours. These models, though, may prove inaccurate in predicting neutral thermospheric density, depending on the level of solar activity, see e.g. (Lathuillère and Menvielle, 2010; Masutti et al., 2016). During times of high magnetic activity, modeled density may underestimate by a factor two the measured one (Sutton et al., 2005). Moreover, some authors (Pardini et al., 2012) found that below 500 km, many atmospheric models overestimated the average atmospheric density by 7% to 20% because of the assumption of a fixed drag coefficient, independent of altitude. An example of how incorrect calculations from empirical models may dramatically affect satellite control, is again the case of the GOCE satellite which, soon after launch, went to safe mode because of what proved a wrong assumption on density levels. Because of the overestimated drag from model, the satellite attitude was bound to rapidly evolve to a critical tumbling condition, with high risk of loss. Different solar indices may prove more apt than others to reproduce thermospheric density, depending on the status of the solar activity. For instance, comparison of EUV proxies in thermospheric density reconstruction at 800 km altitude, from 1997 to 2010, (Dudok de Wit and Bruinsma, 2011) indicated SOHO EUV data as the most suitable to reproduce thermospheric densities at 800 km, during the analysed period. MgII index was also compared to this proxy, showing good, although not optimal, performance, at that altitude.

In our analysis paper, we shall analyse MgII data available for the 2009-2012 period, thus partly overlapping to that data set, although at a very different height. We shall use the low-altitude GOCE data which have become available since that cited analysis (Bruinsma et al., 2014).

2 The Solar Input and thermospheric response

The structure and dynamics of Earth's Thermosphere is controlled by the solar input mainly through the highly variable solar EUV radiation, on the day side. Joule dissipation of induced ionospheric currents and kinetic energy deposition from low energy particles in the auroral zones (Sarris, 2019; Knipp et al., 2004; Qian and Solomon, 2012) also contribute. Geomagnetic activity, that is particles deposition and ionospheric/magnetospheric effects, is triggered by the interaction , with Earth's magnetosphere. The solar wind itself is composed by two components, fast and slow, which may interact with each other during their travel in the interplanetary space, originating shocks impacting the Earth's magnetosphere. The EUV flux accounts on average for about about 80% of this energy input, while the geomagnetic input accounts for the remaining 20%. However, during intense geomagnetic activity, geomagnetic contribution may rise up to about 70% of the energy input (Immel et al., 2004; Lu et al., 1998). The EUV flux has itself a large (up to a factor two) spectrum of variability around its base value (Del Zanna and Andretta, 2011). Thus geomagnetic activity is a variable source of energy and has an impulsive component varying on short timescales of hours, during geomagnetic storms, and a more stable background, away from storms. These fast variations in time, may cause local variation of density of a factor of 2 or three with respect to the pre-event average value, see Figure.4 below. Radiative input from the Sun, instead, has a more continuous character. The 27-day solar rotation period induces changes in the solar emission correlated with the motion of active regions across the Earth-facing solar disk. During the course of the 11-years solar cycle, density is seen to vary by a factor of about 6 at low altitudes (250 km). Seasonal and semi-annual variations are induced by the movement of the sub-solar point and the uneven heating of the two hemispheres at solstices; Diurnal variations are also present, which produce an asymmetry in density between the sun-lit and the dark hemispheres. Thermosphere thus responds to this composite input on many different timescales.

3 Data sets: GOCE Thermospheric density and solar and geomagnetic indices

GOCE, the Gravity field & steady-state Ocean Circulation Explorer (Drinkwater et al., 2003), was launched by ESA on March 17, 2009 to map Earth's gravity field. It has had a 5 year lifetime, flying at the exceptionally low altitude between 260 and 230 km. No other civilian satellite has ever flown this low within the thermosphere **for such an extended time**. GOCE was kept in a drag-free orbit in a dawn-dusk 96.7° sun-synchronous orbit. **Mission profile is shown in Fig. 1. As apparent from the figure, soon after Commissioning GOCE was brought to a mean altitude of 260 km. Nominal Operations then started on September 2009, going on through the end of July 2012. On Aug 1st, 2012, after three years spent flying at nominal altitude, a low-orbit campaign was started for GOCE, steadily bringing its orbit down to 229 km. De-orbing then started on Oct 20 2013 and Satellite was lost few days after. Figure 2 shows the full span of the GOCE thermospheric density dataset in context with Solar Cycle XXIV. The red boxes show how GOCE Mission covers the full rising phase from solar minimum to solar maximum. Three sub-periods have been identified within GOCE Mission time, and selected for subsequent analysis: Low solar Activity phase, from Mission start to end of September 2010; Rising Phase, until July 2012 where activity rises from minimum to maximum level, and a steady, High Activity phase until end of Mission on Nov 2013, where activity is almost stationary and close to Solar Max levels. Comparing with the Mission profile**

timeline, the High Activity period coincides with GOCE's low-orbit campaign. The average value of density is therefore expected to be monotonously rising with time, in this period, due to altitude lowering. Solar activity level is, instead, stationary at the highest levels. Decoupling of the trend due to orbit lowering is therefore possible in density data from this last period..

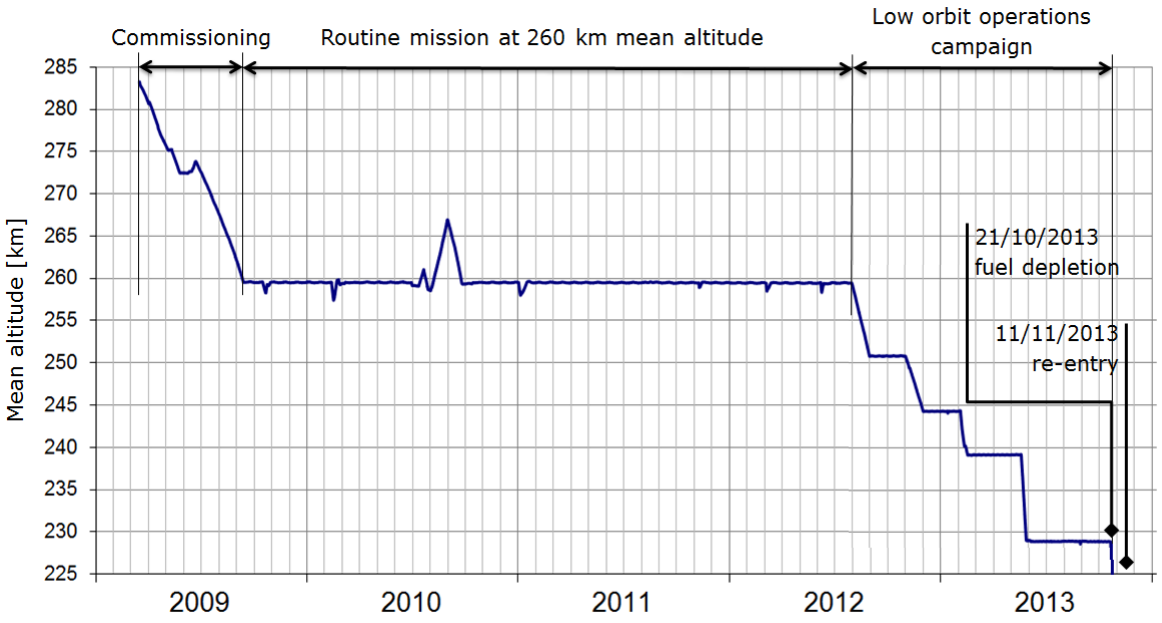

Figure 1. GOCE Mission profile (GOCE Flight Control Team, HSO-OEG, 2011). Low orbit campaign (260-230km height) starts August 1st 2012, through end of Mission, Oct 20, 2013.

To keep the satellite in drag-free mode, extremely sensitive accelerometers were coupled to an ion thruster. Data from the accelerometers has been processed to a thermospheric density dataset (Bruinsma et al., 2014) which has been made available by ESA through the GOCE Virtual Archive (ESA). Data are organized in monthly data files starting from November 1st, 2009 00:00:00 and ending October, 20, 2013 04:07:10 . Sampling rate is 10s. We use Release 1.5 of the dataset. Geomagnetic Ap Index and Solar index F10.7 have been retrieved from NASA Goddard Space Flight Center OMNIWeb interface (Omniweb, 2018). Composite Mg II index v5 dataset have been retrieved from UVSAT of Bremen University Institut für Umweltphysik, (UVSAT, 2018). Sunspot number has been retrieved from SILSO data/image portal of Royal Observatory of Belgium, Brussels.

In the subsequent analysis, solar proxies are tested with their capability to reproduce thermospheric density, within these three different dynamical regimes. **In Fig.3, the full-Mission thermospheric density dataset is shown. Density signal is sampled at 10s and has a periodic, high-frequency, component due to the satellite orbit, lasting 90 minutes. We remove this high-frequency component, shown in the inset of Fig.3, by averaging the signal over one day, that is approximately 16 orbits** Due to in-flight anomalies, the density dataset is affected by gaps, ranging from tens of seconds to days. The most significant gap starts July 8th 2010 and lasts 67 days. Also to be noted is the expected steady increase in average density due

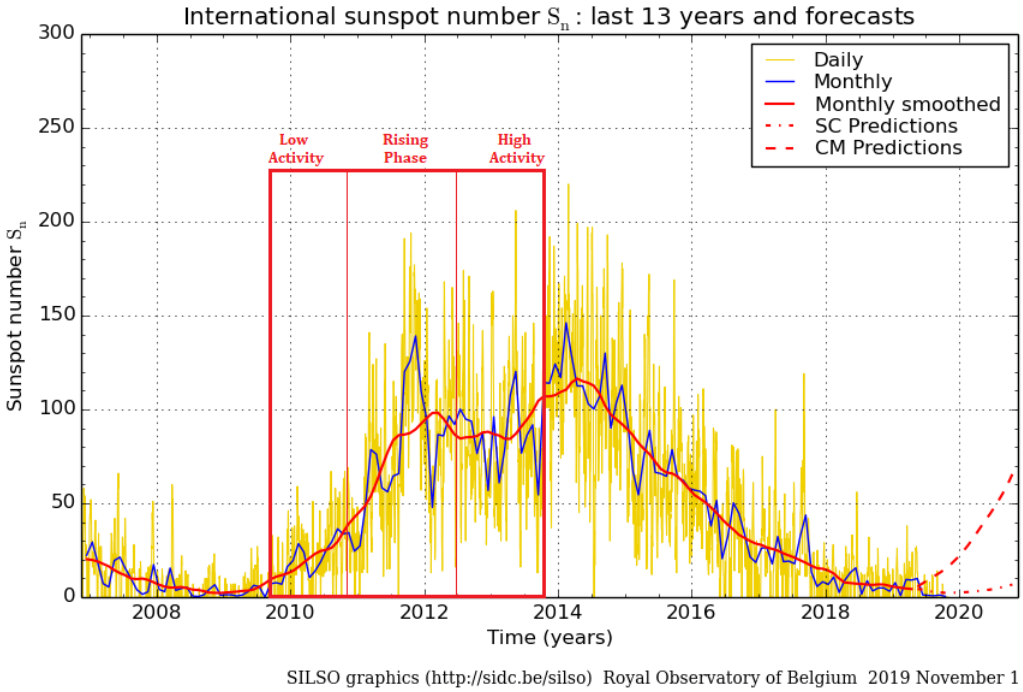

Figure 2. GOCE dataset in context with Solar Cycle 24. The inset shows the data span, further divided into low activity (from Mission start), medium activity (rising phase of cycle 24, from 24/09/2010) and high activity (cycle 24 stationary high-activity phase, from 04/07/2012), which mostly coincides with the altitude lowering phase of the Mission, starting Aug 1st 2012.

to the orbit lowering after July 2012. Signal from solar and geomagnetic proxies, F10.7, MgII and Ap, have been pre-treated for outliers identification and removal. Spline interpolation have been used to fill in missing or removed data. The Ap signal, which is available on a three-hours interval, has been averaged over 24 hours. Ap has also been shifted by a fixed 9-hours amount. The thermosphere, infact, reacts to the impulsive geomagnetic forcing with a delay. We have determined this delay by maximising the correlation between Ap and ρ signals during geomagnetic events, resulting in a fixed 9-hours delay which has been applied to the Ap signal. Geomagnetic storms represent the impulsive component of the solar input, lasting from hours to days. They originate from solar plasma ejected during CME events and impacting Earth's magnetosphere, or from shocks forming at the interfaces between fast and slow solar wind. Figure 4 shows four examples of atmospheric response to geomagnetic storms, occurred during Mission lifetime and captured by GOCE. Reconfiguration of the geomagnetic field induces currents in the ionosphere. Remembering that Ap's sample period is 3 hr, thermospheric response to geomagnetic forcing may indeed be between six and twelve hours. Fig. 4 also shows (see e.g. top left panel) how thermospheric response is not only delayed, but relaxes to the quiet state with a finite characteristic time of the order of one day. Thus, a second event happening during relaxation (see e.g. bottom left panel), will add up to the first one, not yet relaxed, resulting in an enhanced value of the thermospheric density (see e.g. panel b). This memory effect is not included in our model which only

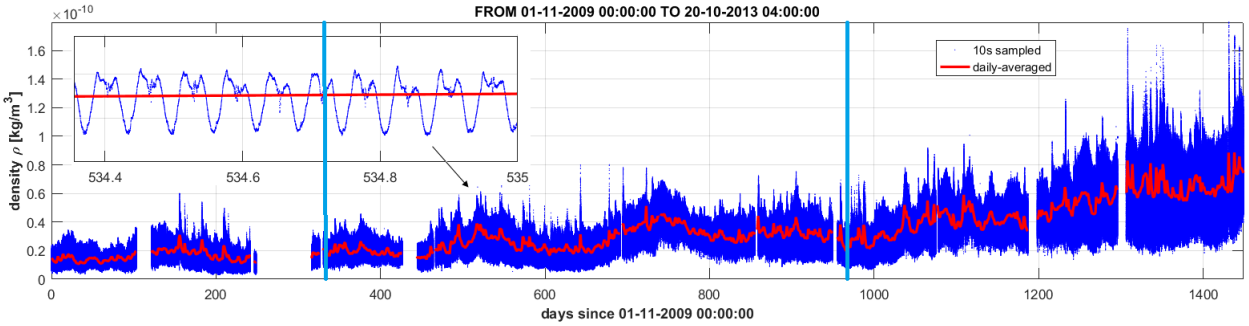

Figure 3. Thermospheric Density from GOCE data. Density profile, provided at 10s sampling rate (blue line), is averaged over one day (red line). In the inset sub-plot, a time span of only 10 orbits is plotted. The periodic, high-frequency fluctuations of density are due to satellite orbit, lasting around 90 minutes. In the main plot, day 0 is start of Operations (01/11/2009). Blue vertical lines at day 327 (24/09/2010) and 976 (04/07/2012) indicate the limits of the three sub-dataset of low, rising and high solar activity, see also Figure 2. Low-orbit campaign starts at day 1004 (01/08/2012), almost completely overlapping with low-orbit campaign. The RSS error in density (not shown) is also provided in the dataset, setting at a level two orders of magnitudes lower than average density.

considers a mean time lag between storms and thermospheric density enhancement. A dynamical model may be constructed, also accounting for relaxation, see e.g. (Dudok de Wit and Bruinsma, 2011), which may better fit multiple impulsive events, more characteristic of high solar activity phases, close to solar Maximum.

Fig.5 shows the evolution of Full-mission Thermospheric density, together with that of solar indices Ap, F10.7 and MgII. It is apparent from the figure, how geomagnetic index Ap does not capture the overall trend due to the rising solar cycle, describing only impulsive events. MgII and F10.7, better follow the long-term trend of thermospheric density. Both F10.7 and MgII over-represent modulations due to solar rotation (see e.g. the main modulation during days 800 to 1000) than thermospheric density does. Correlation, though, is apparent. As expected, very poor average correlation is shown by ρ and Ap , due to the intermittent nature of the geomagnetic input. Correlation between ρ and solar fluxes is instead clear, being higher in times of low solar activity, that's for low values of F10.7 and Mg II. In times of high solar activity (high values of F10.7 and Mg II), correlation with solar fluxes gets worse. MgII tends to be better correlated than F10.7 at average values of thermospheric density, confirming the role of UV flux in coupling with the thermosphere. A Correlation coefficient

$$R_{xy} = \frac{\sigma_{xy}}{\sigma_x \sigma_y} \tag{1}$$

may be calculated between the variables $\rho; F10.7$ and $\rho; MgII$, resulting in a value of $R_{\rho,F10.7} = 0.57$ and $R_{\rho,MgII} = 0.67$, respectively, indicating a better overall correlation between thermospheric density and MgII index, with respect to F10.7. EMD analysis below, will further clarify the interplay of the various indices to reproduce the density fluctuations.

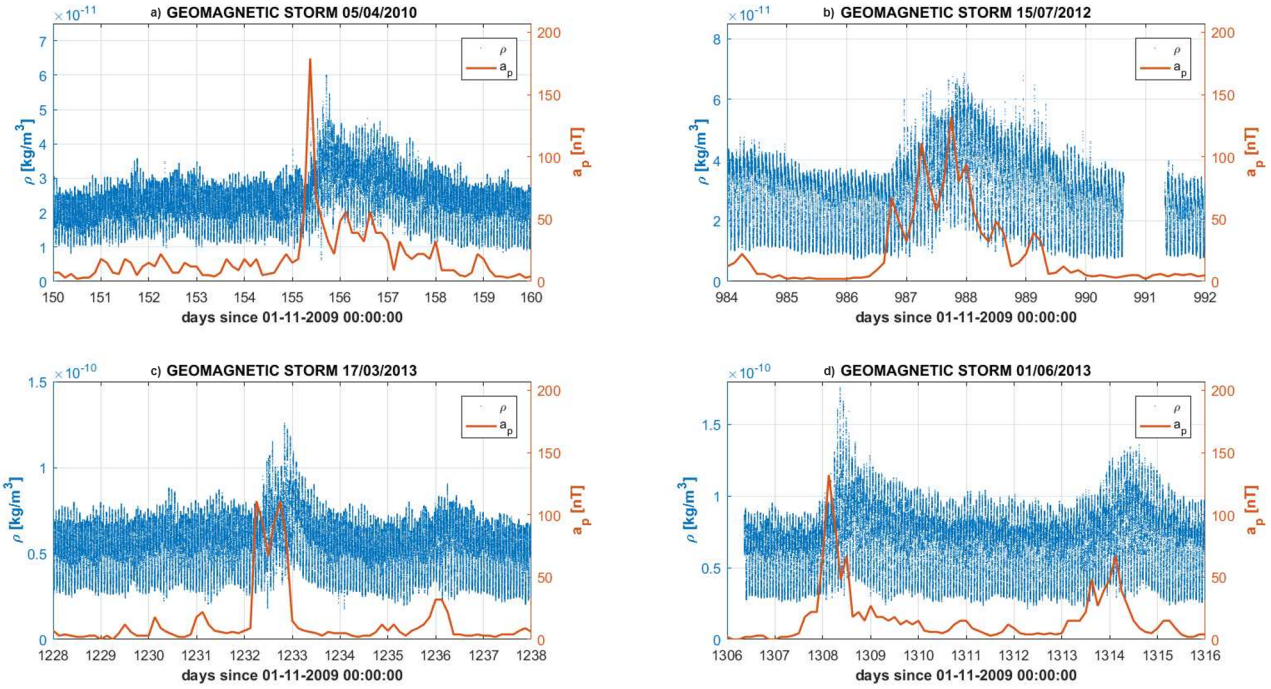

Figure 4. Thermospheric density ρ (blue line) and a_p index (red line) during four geomagnetic storms occurred in the course of the GOCE mission. From Top-Left to Bottom-Right: a) 05/04/2010 [day 155]; b) 14/07/2012 [day 986]; c) 13/03/2013 [day 1232]; d) 01 and 07/06/2013 [days 1308 and 1314]

4 Data analysis and density synthesis from proxies

Time series from the solar proxies result from non-stationary and nonlinear problem. Standard signal-processing analysis tool such as harmonic decomposition or wavelet analysis, are not suited to extract relevant features from Sun-related time series (Lovric et al., 2017). Empirical Mode Decomposition (EMD) (Huang et al., 1998) will be used for analysing all time series in this paper. EMD decomposes a signal as a sum of a finite number of basis funcion called Intrinsic Mode Functions(IMFs). These are generated iteratively by constructing successive envelopes of the signal and than removing this envelop and iterating. This process returns global modes (as opposed to wavelets which are local modes) which are non-periodic (as opposed to Fourier base functions) and with almost zero mean value. IMFs are representative of trends embedded in the signal with a time-variable amplitude and frequency, yet still characterized by a typical scale-length. Lowest modes are associated with the highest temporal variability. The highest mode is the global trend. IMFs are given in the time-domain and are defined in the full time domain as the original dataset. The algorithm defining the IMF technically consists in a series of steps (called sifting) whereby all local extrema (minima and maxima) of a signal x(t) are identified; local minima are then interpolated by cubic spline to get a lower envelope $e_{min}(t)$. A similar procedure on maxima defines an upper envelope $e_{max}(t)$. A mean envelope $m(t) = [e_{min}(t) + e_{max}(t)]/2$ is then calculated,

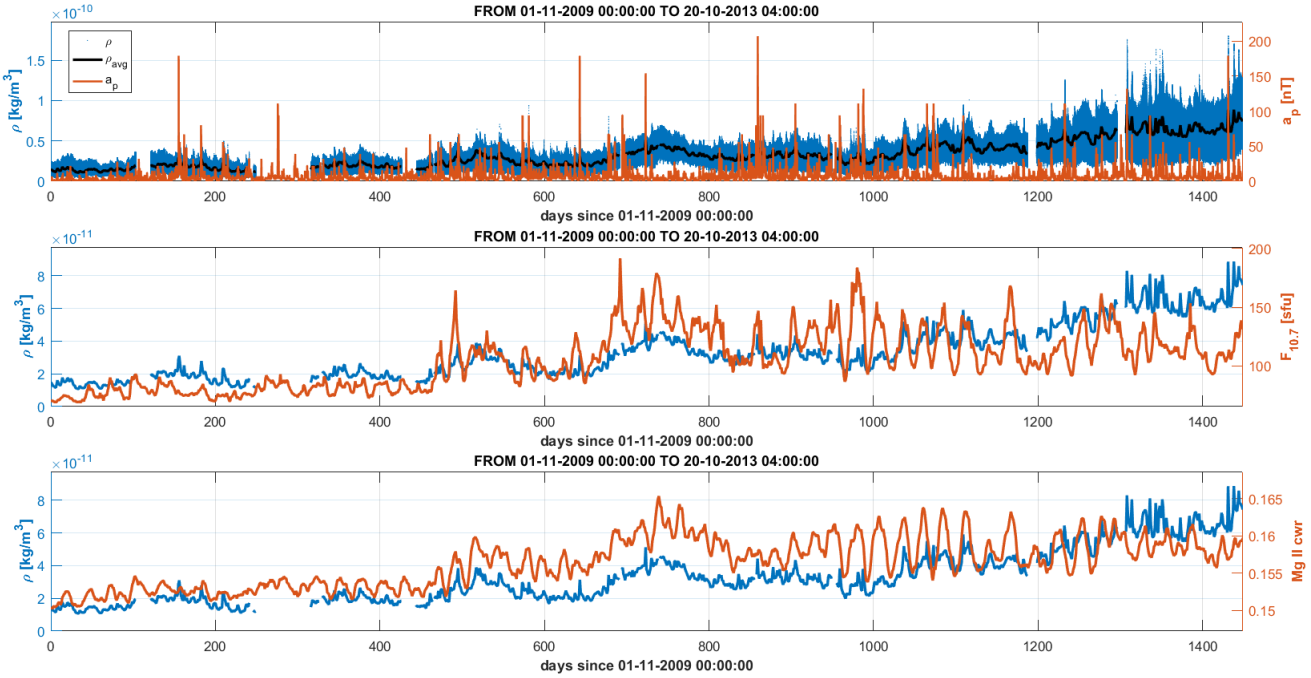

Figure 5. Comparison of time series for full-mission thermospheric density, and solar indices Ap, F10.7 and MgII. Top panel: density (full dataset, blue line, and daily averaged, black line) with the Ap index (red line). Middle and bottom panels: daily averaged density (blue) and F10.7 and MgII indices (red), respectively.

returning the low-frequency part of the original signal x(t). This process is iterated, starting from a new signal obtained by removing the mean envelope m(t) from the original signal $h(t) = x(t) - m(t)$. In this way, a set of IMF's containing the highest frequency features is obtained first. Iteration is than carried on, defining more IMP's, until the residual between signal and the IMF, becomes a monotonic function from which no furhter IMF can be extracted. Figures 7-9 show the full set of IMF's in the EMD decomposition for solar proxies' time series.

5 Results

Solar proxies are analysed and the resulting set of IMF's are reported in Figures 7-9. Lowest order IMF's are associated with the most rapidly varying components of the signal while the residual captures the overall trend. The number of IMF's is not fixed a-priori and depends on the convergence criterion chosen for stopping the EMD algorithm.

Thermospheric density signal is then reconstructed from a linear superposition of the set of IMF's from the solar proxies:

$$\bar{\rho} = N[A^{A_p} \cdot \sum_i c_i^{Ap} IMF_i^{A_p} + A^{F_10.7} \cdot \sum_i c_i^{F10.7} IMF_i^{F_10.7} + A^{MgII} \cdot \sum_i c_i^{MgII} IMF_i^{MgII}] \quad (2)$$

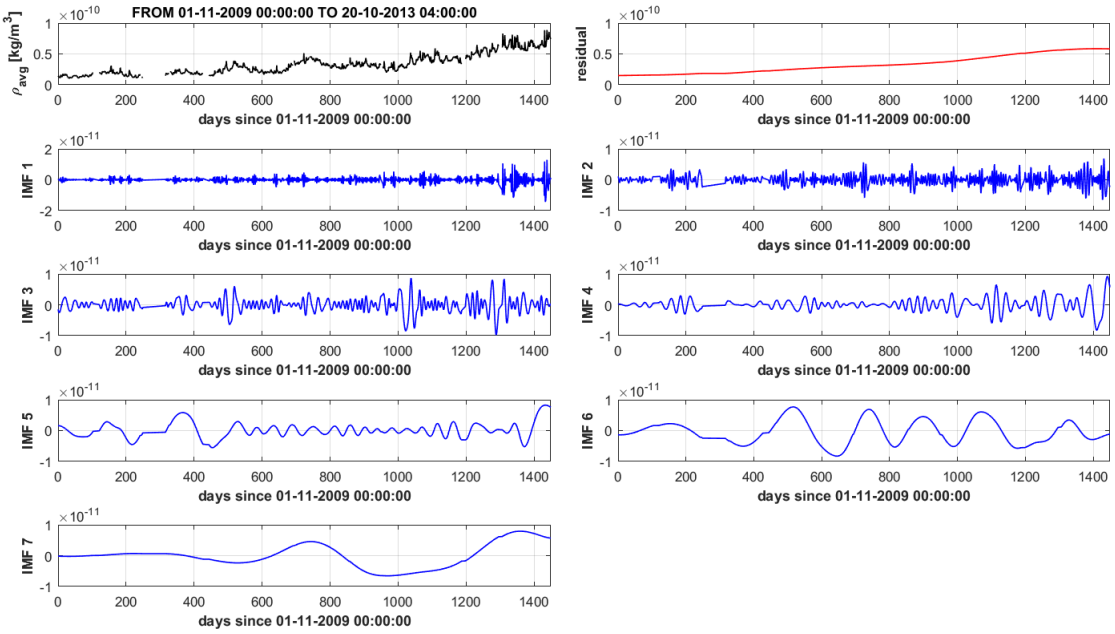

Figure 6. EMD decomposition for the thermospheric density signal from GOCE data, 2009-2013. Top row: original signal and trend. From row 1, successive orders of basis finctions (IMF's)

where the coefficients c_i may be zero or one, thereby selecting only a subset of the IMF components function resulting from the signal analysis. We have determined the optimal combination of IMF's, capable of reproducing the signal, based on the minimization of the RMS error:

$$\sigma_{RMS} = \sqrt{\frac{1}{N}\sum_{i=1}^{N}(\rho - \bar{\rho})^2}$$

Fig.10 shows the best synthesised signal from a combination of the Full-Mission IMF modes from Ap , MgII and F10.7 Fig. 11 shows instead the best synthesised signals from the different sets of IMF's determined for the three separate subsets, during low solar activity, rising phase and high solar activity. Table 1 shows, for all cases, the individual components of the optimal synthesized signal. Table 2 compares the optimal solution with two cases where either F10.7 or MgII is selected as solar UV proxy. A number of consideration may be drawn from the analysis. Firstly, all syntheses require the A_p signal to be taken into account, although during low solar activity its amplitude and therefore its relative contribution to the overall signal is small. This confirms the relevance of the state of the interplanetary medium on the short-term dynamics of the thermosphere. The A_p signal is intermittent and all IMF components are always needed to reconstruct the signal. This is not the case for the solar flux proxies, F10.7 and MgII, whose long-wavelength components appear most in the decomposition for all periods. The solar input is therefore basically captured, on the short-time-scale, by the variations of the geomagnetic input captured by A_p, and on the longer timescales by the proxies of the solar radiative flux, F10.7 and MgII. **During the rising phase of the solar cycle**

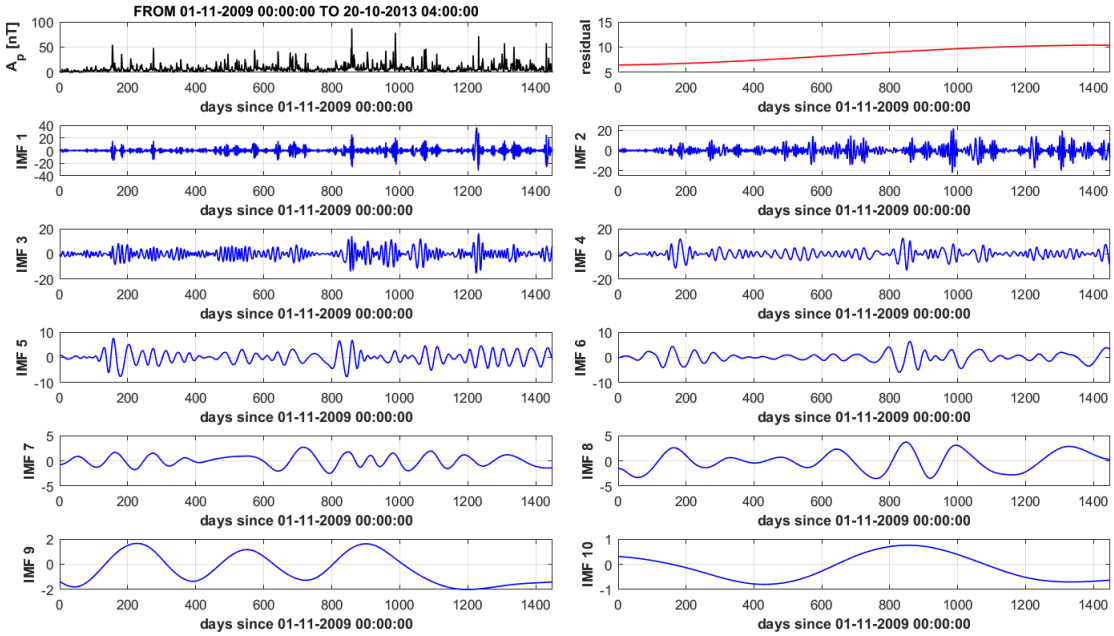

Figure 7. EMD decomposition for the geomagnetic index Ap. Top row: original signal and trend. From row 1, successive orders of basis finctions (IMF's)

and during high solar activity period, the contribution of the geomagnetic proxy A_p has a much higher amplitude than during low activity and the contribution to density of changes in the interplanetary medium is therefore dynamically relevant. Another conclusion which can be drawn is that the $MgII$ index performs better then the $F10.7$ one. In fact, the sole combination of A_p and $MgII$ is performing very similarly to the full three-indices combination. The only exception being low solar activity periods, where inclusion of $F10.7$, somewhat improves signal reconstruction.

We have seen earlier how low-orbit operations overlap with the period of high solar activity. A rising trend in average density is therefore apparent in Fig.10, due to density increase because of orbit lowering. This rising trend could not be captured by the solar indices, in the same figure. However, if de-trended, in the third period data show as in Fig.12, where the rising trend is no more seen and agreement of the two curves is on the same level as in the previous period of rising solar activity: Table 1 reports the values of the RMS error in the high activity period for the original and the de-trended density signal, showing a decrease from 14% to 11% when accounting for density increase due to orbit lowering.

6 Conclusions

We have performed an analysis of three of the most commonly used solar flux and geomagnetic proxies, F10.7, MgII and A_p in relation to the time evolution of thermospheric density measured in-situ from 260 to 230 km altitude, using the GOCE

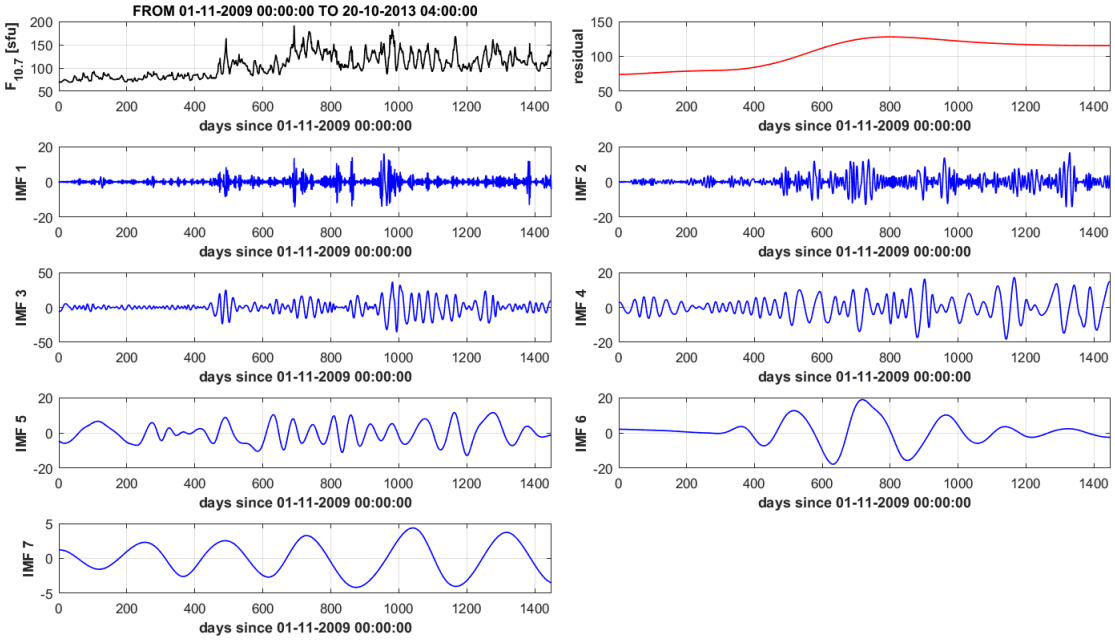

Figure 8. EMD decomposition for the F10.7 solar radio flux. Top row: original signal and trend. From row 1, successive orders of basis finctions (IMF's)

Table 1. Components of optimal synthesized signal, for the case of full mission, low, rising and high solar activity during Cycle 24. RMS error σ_{RMS} (normalized to the mean value) and component amplitudes, A.

Dataset	$\sigma_{RMS}[\%]$	Index	1	2	3	4	5	6	7	8	9	10	Residual	A
		A_p	x	x	x	x	x	x		x	x		x	1
Whole Mission	11	$MgII$	x			x		x	x				x	6.7
		A_p	x	x	x	x	x	x	x	x	x	x	x	1
Low Solar Activity	2.6	$F10.7$		x				x					x	11
		$MgII$					x	x		x			x	12
		A_p	x	x	x	x	x	x	x				x	1
Rising Solar Activity	7.4	$F10.7$	x	x									x	0.35
		$MgII$	x			x		x	x				x	5.1
		A_p	x	x	x	x	x	x	x	x		x		1
Max Solar Activity	14	$MgII$							x				x	7
	(11 if de-trended)													

thermospheric density dataset, which spans most of the rising phase of Solar cycle 24, from minimum to maximum, covering the full dynamical spectrum of the solar input of the thermosphere. Thermospheric density signal, for the whole Mission and

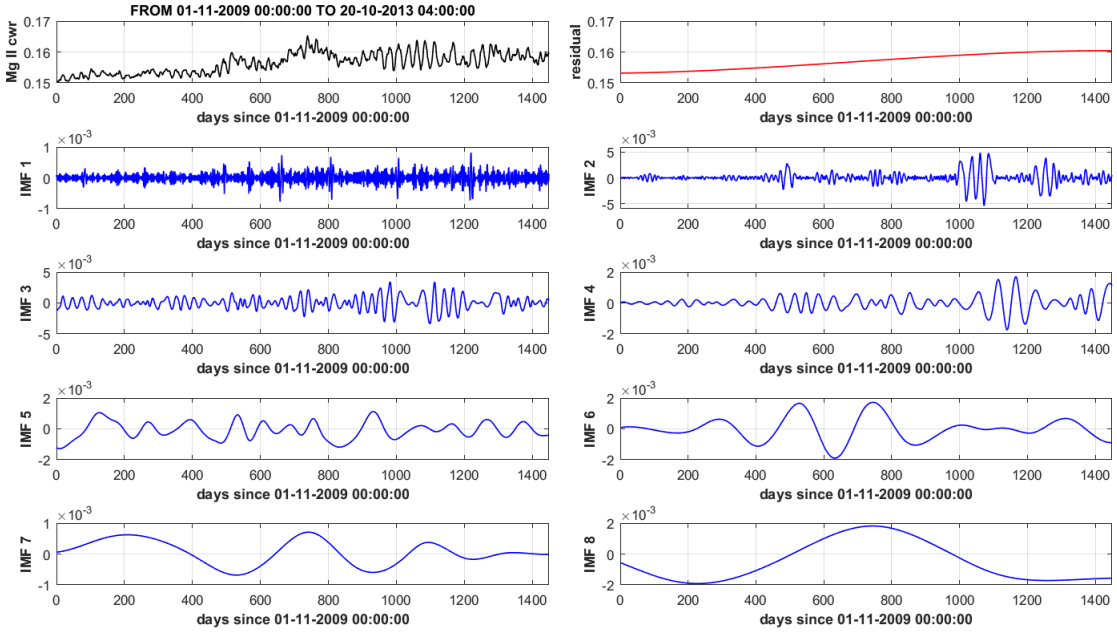

Figure 9. EMD decomposition for the MgII solar UV flux proxy. Top row: original signal and trend. From row 1, successive orders of basis finctions (IMF's)

Table 2. Comparison of normalised RMS errors (in %) for different optimal combinations of proxies

Solar activity level	$A_p + MgII + F10.7$	$A_p + MgII$	$A_p + F10.7$
Whole Mission	11	11	14
Low	2.6	3.1	3.3
Rising	7.4	7.4	8.3
Max	14	14	16

form three sub-intervals of low, rising and high solar activity, has been analysed through Empirical Mode Decomposition. Once the basis functions have been determined, they have been optimally recombined to reconstruct the density signal. **Analysis shows how the geomagnetic proxy A_p is always needed to capture the impulsive short-term features of the density signal connected with the evolution of the interplanetary medium. However, during low solar activity, Ap contribution has a much lower amplitude than the other signals. Thermospehric density in this period is therefore driven by the low-frequency variations of the radiative input, captured by the solar flux proxies F10.7 and MgII. A lesser contribution comes from the drive of the interplanetary medium impacting Earth. During the rising phase of the solar cycle and during high solar activity period, the contribution of the geomagnetic proxy A_p has a much higher amplitude than during low activity and the contribution to density of changes in the interplanetary medium is therefore dynamically relevant.** During low and medium solar activity, thermospheric signal can be reconstructed with an RMS errors of about 2.6%

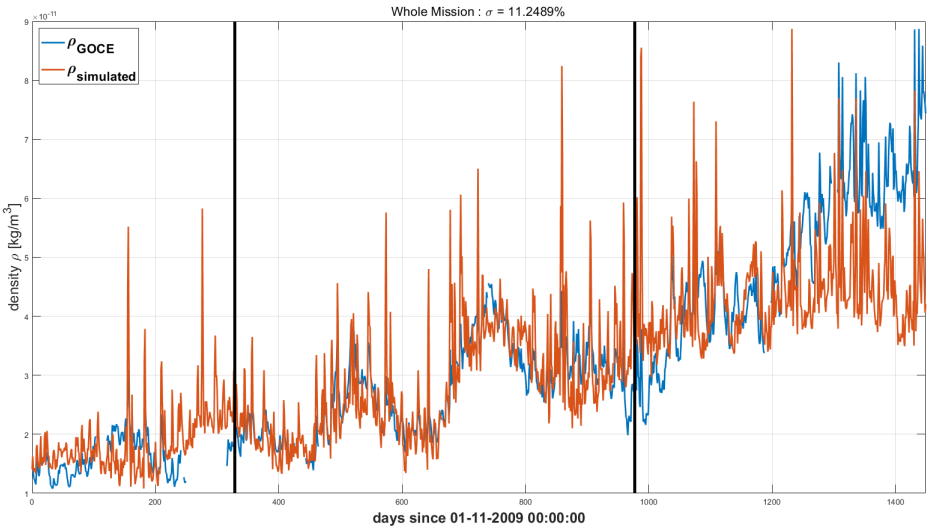

Figure 10. Thermospheric density synthesized (red line) from optimal combination of A_p , MgII and F10.7. Whole Mission. Blue line shows thermospheric density data. The rising trend in density the last third of the Mission time is due to orbit lowering and is therefore not showing in the reconstructed signal.

and 7.4%, respectively. Semi-empirical atmospheric models (NRLMSISE-00 and Jacchia-family models above all) are usually credited to fall in the 10% error range. During high solar activity, error increases to 14%, **but this figure is worsened by the steady rising trend in mean density due to orbit lowering, not present in the solar input, and is therefore over-estimated. If de-trended,the signal shows an rms value, in the third period, of 11%. The selection of the optimal combinations, which we have presented in this paper, is instead independent on the absolute value of the rms error.** MgII, proves to be a better proxy than $F_10.7$ in capturing the long-term trends of the solar input during the solar cycle and is therefore to be preferred when only the long-term trend is of interest. Combining Ap (shifted by 6 hours to take into account thermosphere's dynamical response to the solar input), and the slowest varying EMD modes from the MgII, returns a good representation of the thermospheric density signal at low thermospheric altitudes. **A final comment should be addressed to the forecasting capability of the reconstruction of density from solar proxies, for different altitudes. Thermospheric density changes by orders of magnitude between 250 and 800 km, that is the portion of our thermosphere where most LEO satellites fly. In this paper we have followed the long term evolution of density at 260 km, rising by almost one order of magnitude through the solar cycle. Extrapolating our results to 800 km altitude would need a self-consistent thermospheric model at different altitudes which is not yet established. On the other hand, constraining current models with datasets at different heights looks a necessary step to be done, and GOCE dataset may be instrumental to such a program.**

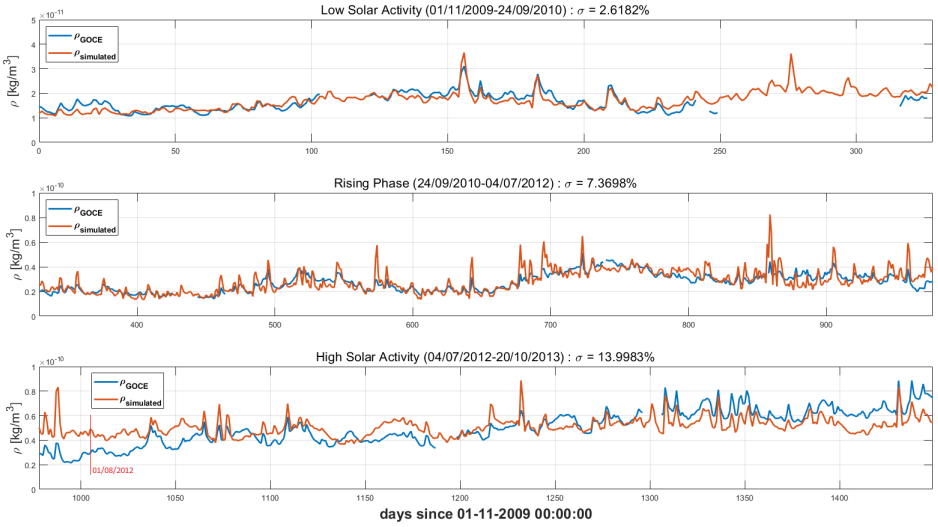

Figure 11. Optimal synthesized Thermospheric density from A_p , MgII and F10.7. Three different EMD sets for the full Mission extent, each covering one of the three selected dynamical activity regimes for Solar Cycle XXIV, low, rising and high. The trend in density apparent in panel three, representing the high solar activity phase, is due to orbit lowering and is therefore not showing in the reconstructed signal.

Code availability. N/A

Data availability. All datasets have been referenced into the main text

Code and data availability. Processing software is based on standard Matlab routines

Sample availability. N/A

Video supplement. N/A

Author contributions. AB:Conceptualization, Writing – Original draft; CC: Data analysis, Software; FB: Methodology, Supervision, Writing – review and editing;

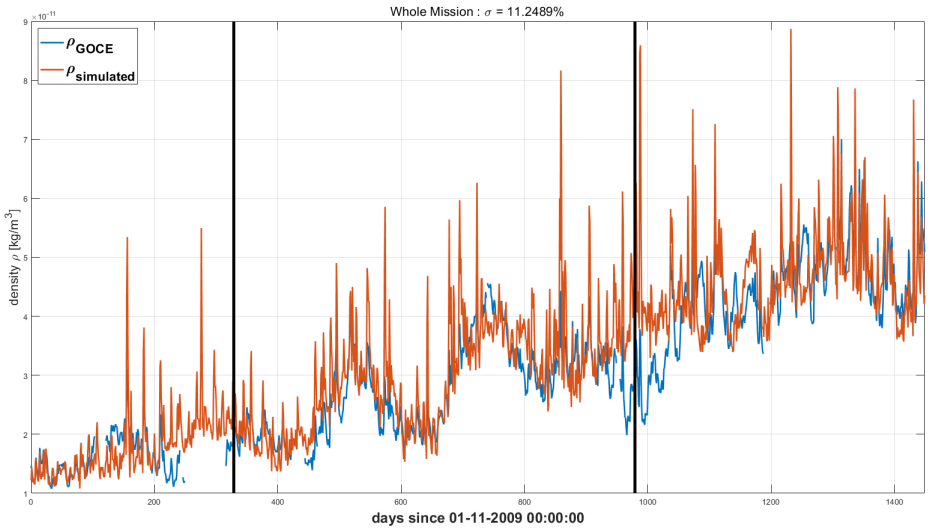

Figure 12. Effect of orbit lowering on the third, high solar activity period, Aug, 1st 2012. Density data (blue line), as shown in Figure 10, have been de-trended to subtract the contribution due to orbit lowering. Red line shows synthesized Thermospheric density values from the optimal combination of A_p, MgII and F10.7. Whole Mission.

Competing interests. The authors declare that they have no conflict of interest.

Acknowledgements. CC aknowledges funding from the Master in Space Science and Technology Master run by the Science "Macro-area", University of Tor Vergata, Rome (IT)

References

Bowman, B. R., Tobiska, W. K., Marcos, F., and Huang, C.: The Thermospheric Density Model JB2008 using New EUV Solar and Geomagnetic Indices, in: 37th COSPAR Scientific Assembly, vol. 37, p. 367, 2008.

Bruinsma, S. L., Doornbos, E., and Bowman, B. R.: Validation of GOCE densities and evaluation of thermosphere models, Advances in Space Research, 54, 576–585, https://doi.org/10.1016/j.asr.2014.04.008, 2014.

Del Zanna, G. and Andretta, V.: The EUV spectrum of the Sun: SOHO CDS NIS irradiances from 1998 until 2010, , 528, A139, https://doi.org/10.1051/0004-6361/201016106, 2011.

Drinkwater, M. R., Floberghagen, R., Haagmans, R., Muzi, D., and Popescu, A.: VII: CLOSING SESSION: GOCE: ESA's First Earth Explorer Core Mission, , 108, 419–432, https://doi.org/10.1023/A:1026104216284, 2003.

Dudok de Wit, T. and Bruinsma, S.: Determination of the most pertinent EUV proxy for use in thermosphere modeling, , 38, L19102, https://doi.org/10.1029/2011GL049028, 2011.

ESA: GOCE Thermospheric data, http://eo-virtual-archive1.esa.int/GOCE-Thermosphere.html.

Floyd, L., Newmark, J., Cook, J., Herring, L., and McMullin, D.: Solar EUV and UV spectral irradiances and solar indices, Journal of Atmospheric and Solar-Terrestrial Physics, 67, 3–15, https://doi.org/10.1016/j.jastp.2004.07.013, 2005.

GOCE Flight Control Team, HSO-OEG: GOCE End-of-Mission Operations Report, https://earth.esa.int/documents/10174/85857/2014-GOCE-Flight-Control-Team.pdf, 2011.

Huang, N. E., Shen, Z., Long, S. R., Wu, M. C., Shih, H. H., Zheng, Q., Yen, N. C., Tung, C. C., and Liu, H. H.: The empirical mode decomposition and the Hilbert spectrum for nonlinear and non-stationary time series analysis, Proceedings of the Royal Society of London Series A, 454, 903–998, https://doi.org/10.1098/rspa.1998.0193, 1998.

Immel, T. J., Sutton, E. K., Nerem, R. S., Forbes, J. M., Mende, S. B., and Frey, H. U.: An investigation of thermospheric neutral density vs.O/N_2 during the Oct-Nov 2003 magnetic storms, AGU Fall Meeting Abstracts, SA23A-0380, 2004.

Knipp, D. J., Tobiska, W. K., and Emery, B. A.: Direct and Indirect Thermospheric Heating Sources for Solar Cycles 21-23, , 224, 495–505, https://doi.org/10.1007/s11207-005-6393-4, 2004.

Lathuillère, C. and Menvielle, M.: Comparison of the observed and modeled low- to mid-latitude thermosphere response to magnetic activity: Effects of solar cycle and disturbance time delay, Advances in Space Research, 45, 1093–1100, https://doi.org/10.1016/j.asr.2009.08.016, 2010.

Lovric, M., Tosone, F., Pietropaolo, E., Del Moro, D., Giovannelli, L., Cagnazzo, C., and Berrilli, F.: The dependence of the [FUV-MUV] colour on solar cycle, Journal of Space Weather and Space Climate, 7, A6, https://doi.org/10.1051/swsc/2017001, 2017.

Lu, G., Baker, D. N., McPherron, R. L., Farrugia, C. J., Lummerzheim, D., Ruohoniemi, J. M., Rich, F. J., Evans, D. S., Lepping, R. P., Brittnacher, M., Li, X., Greenwald, R., Sofko, G., Villain, J., Lester, M., Thayer, J., Moretto, T., Milling, D., Troshichev, O., Zaitzev, A., Odintzov, V., Makarov, G., and Hayashi, K.: Global energy deposition during the January 1997 magnetic cloud event, , 103, 11 685–11 694, https://doi.org/10.1029/98JA00897, 1998.

Masutti, D., March, G., Ridley, A. J., and Thoemel, J.: Effect of the solar activity variation on the Global Ionosphere Thermosphere Model (GITM), Annales Geophysicae, 34, 725–736, https://doi.org/10.5194/angeo-34-725-2016, 2016.

Omniweb, N.: Geomagnetic Ap Index from NASA Omniweb archive, https://omniweb.gsfc.nasa.gov/form/dx1.html, 2018.

Pardini, C., Moe, K., and Anselmo, L.: Thermospheric density model biases at the 23rd sunspot maximum, Planetary and Space Science, 67, 130–146, https://doi.org/10.1016/j.pss.2012.03.004, 2012.

Picone, J. M., Hedin, A. E., Drob, D. P., and Aikin, A. C.: NRLMSISE-00 empirical model of the atmosphere: Statistical comparisons and scientific issues, Journal of Geophysical Research (Space Physics), 107, 1468, https://doi.org/10.1029/2002JA009430, 2002.

Qian, L. and Solomon, S. C.: Thermospheric Density: An Overview of Temporal and Spatial Variations, , 168, 147–173, https://doi.org/10.1007/s11214-011-9810-z, 2012.

Sarris, T. E.: Understanding the ionosphere thermosphere response to solar and magnetospheric drivers: status, challenges and open issues, Philosophical Transactions of the Royal Society of London Series A, 377, 20180 101, https://doi.org/10.1098/rsta.2018.0101, 2019.

SORCE: MgII cwr Index from SORCE Experiment, http://lasp.colorado.edu/data/sorce/ssi_data/mgii/txt/sorce_mg_latest.txt, 2018.

Sutton, E. K., Forbes, J. M., and Nerem, R. S.: Global thermospheric neutral density and wind response to the severe 2003 geomagnetic storms from CHAMP accelerometer data, Journal of Geophysical Research (Space Physics), 110, A09S40, https://doi.org/10.1029/2004JA010985, 2005.

UVSAT, B.: Observations of solar activity by GOME, SCIAMACHY, and GOME-2, Institut für Umweltphysik - Universit at Bremen, http://www.iup.uni-bremen.de/UVSAT/Datasets/mgii, 2018.